An investigation of the contribution of structural modes, a Helmholtz resonance, and a nonlinear harmonic to the directional behavior of Balinese gamelan gongs

Dallin Harwood

A capstone report submitted to the faculty of
Brigham Young University
in partial fulfillment of the requirements for the degree of

Bachelor of Science

Dr. Micah Shepherd, Advisor

Department of Physics and Astronomy

Brigham Young University

ABSTRACT

An investigation of the contribution of structural modes, a Helmholtz resonance, and a nonlinear harmonic to the directional behavior of Balinese gamelan gongs

Dallin Harwood
Department of Physics and Astronomy, BYU
Bachelor of Science

Balinese gamelan gongs are percussion instruments of special interest because of their unique geometry and sound. Unlike a Chinese tam-tam, the gongs are quite thick, with a protruding dome in the center and long edges that sharply wrap around the circumference of the gong. When struck in the center, the larger gongs are designed to produce a strong beating effect. Previous studies have shown the cause of this beating phenomenon to be the proximity of the harmonic of the first axisymmetric mode to the frequency of the second axisymmetric mode [1]. The work presented in this thesis includes three studies that characterize the directivity of the instrument. First, scanning laser Doppler vibrometer (SLDV) measurements were taken alongside directivity measurements to demonstrate the connection between operating mode shapes and far-field behavior. In most cases the antinodal regions along the circumference of the operating mode shape matches the number and location of lobes in the directivity plots. The directional and vibrational characteristics of a large and small gong were compared to show differences between them. Second, physical measurements and application of a model identified a Helmholtz resonance in the cavity of a large gong. The cavity resonance dominates far-field behavior for neighboring frequencies. And third, excitation of the gong using the first and second axisymmetric mode frequencies provided insight into the nonlinear harmonic that causes the beating. The harmonic behaved like the second mode of the fundamental in both directivity and vibration, implying its vibration is not limited to the shape of only the first axisymmetric mode but the nonlinear effects could complicate the mode behavior with influence from higher order modes.

Keywords: beating, directivity, harmonic, Helmholtz resonator, modeling, musical acoustics, nonlinear, vibrational modes

ACKNOWLEDGMENTS

I would like to express gratitude to Samuel Bellows and Dr. Kent Gee for the introduction to the physics of the gamelan gongs. I'm grateful to Dr. Gee who served as my original advisor on this project, and to Dr. Micah Shepherd for the many months since that he has advised me and helped me become a better experimentalist. I'm also grateful to Hanna Pavill, Micah Hattaway, Emma Todd, and Joseph Avila who assisted with measurements, and Jeremy Peterson who constructed installations for the gong and shaker. I thank Dr. Jeremy Grimshaw for providing the instruments and cultural background information as well as Dr. Matt Allen for providing the shaker used for higher amplitude excitation and for his insightful comments. The BYU College of Computational Mathematical and Physical Sciences provided funding for these projects.

Contents

List of Figures

List of Tables

Chapter 1

Introduction

Balinese gongs are uncommon in western orchestras, yet they form a key part of Indonesian culture, both musically and spiritually. This introduction details some of the characteristics of a Balinese gamelan and specifically comments on individual instruments. It presents several studies on topics including musical instrument directivity and measurements of gamelan instruments. Finally, a short introduction to the current work provides a connection between the studies presented in this thesis and those done previously.

1.1 Cultural Background

Bali is an island province of Indonesia near Java. Its culture is full of intricacies, including many calendars and extreme attention to detail in clothing, architecture, and music. The Balinese gamelan is at the heart of music in Bali. The gamelan, meaning ensemble, contains anywhere from a few to as many as over seventy percussion instruments, including metallophones, drums, and gongs [1]. In Bali, the definition of an octave is different from that in Western music, creating a distinctive sound. Instruments are often made in pairs, where a brother and sister bar on a metallophone are tuned slightly off pitch from each other, creating acoustic beating when struck in unison. This beating

creates a shimmering quality to the music of the gamelan referred to as "ombak," literally meaning "wave." In Balinese music, the metallophones typically play melodies and harmonies, while drums play syncopated rhythms and the gongs establish strong and weak beats in the meter or are left to ring at the end of a phrase [2].

The gongs of the gamelan are especially unique because the larger gong ageng, or "great gongs," produce beating independently. The gong ageng consist of the gong wadon, a "female" gong with an 83 cm diameter, and the "male" gong lanang with an 82 cm diameter. These two gongs beat when struck on the boss, which is the polished golden dome in the center of the gong. The gong kempur (or kempul) and the bebende are smaller gongs and do not produce beating. The bebende is played with a small wooden hammer, as opposed to the soft mallet used on the other gongs, and is usually played with more syncopation. Other "pot" gongs are fixed horizontally on taut strings rather than hung, and are played with wooden mallets.

Figure 1.1 The Balinese gamelan gong ageng. The lanang and wadon are hung on the left and right respectively with the gong kempur in the center and a smaller gong in front. The golden boss in the center of the three large gongs is prominent, and the significant length of the sides is visible. The geometry is quite different from a Chinese tam-tam with more complications resulting from the hand crafted nature of the instruments [3].

Unlike the Chinese tam-tam, these gongs are more tonal and have completely different geometries as seen in Figure 1.1. The golden boss is striking, protruding several centimeters on all the gongs except the bebende which is nearly flat (as seen in Figure 2.1). The gongs also have a significant depth, with the edge wrapping backward nearly half the length of the radius. The thickness of the gongs varies as they are meticulously crafted by hand (traditionally out of bronze) with an average thickness of 5mm near the boss and 3mm on the face and rim.

1.2 Previous Studies

The directivity of a musical instrument characterizes its style and use. For example, musicians and acousticians understand that brass instruments with bells are extremely directional at higher frequencies, whereas woodwinds and strings are less so due to the nature of those instruments. Low frequencies in orchestral instruments exhibit more omnidirectional behavior and Meyer concluded that this type of radiation occurs primarily below 500 Hz, with more complex behavior above 500 Hz [4]. The study by Meyer also discusses the effect of room acoustics on how sound is perceived from a group of musicians and how the seating arrangement of the musicians themselves can change the overall directivity of an orchestra.

Although western instruments have been the focus of most musical acoustics studies, there are some exceptions, notably Fletcher and Rossing [5]. In *The Physics of Musical Instruments,* a summary of different percussion instruments is given, including Balinese gongs. A study of a large gong and a tawa tawa demonstrated the acoustic importance of the first three modes at different times after a strike. They explain that the first two axisymmetric modes have a near 2:1 octave ratio, which is a deliberate feature caused by the mass of the boss. An explanation of circular plates is also given in the book, which is essential for understanding the basic vibration patterns of the gongs. Fletcher and Rossing provide tables of possible mode shapes, notated with m nodal diameters and n

radial nodes (m,n). The convention used in this thesis begins with the lowest-order mode written as (0,1).

The nonlinear behavior of shells, tam-tams and gongs has also been researched. Chaigne et al. studied partial shells and compared their nonlinear behavior to that of the Chinese tam-tam [6]. They confirmed the presence of harmonics in the shells with values from the sum or difference of the first frequencies ($f = f_1 \pm f_2$) or an integer multiple of the fundamental ($f = n * f_1$). They also observed that the imperfections in the gongs cause a shift in the arrival of axisymmetric modes and the distance between degenerate modes. Degenerate modes occur much closer together in the symmetric manufactured shells and the axisymmetric modes happen at lower frequencies than they do in the tam-tam.

Several other studies have focused on instruments in the Balinese gamelan. Jones et al. studied the vibrational characteristics of the metallophones in the gamelan and contrasted them with a glockenspiel [7]. A study by Perrin et al. investigated the normal modes of a small gamelan gong [8]. They applied finite element method (FEM) modeling, electronic speckle pattern interferometry (ESPI), and scanning laser doppler vibrometry (SLDV) to record the structural response of the gong. They noted a fixing of the nodal lines, likely due to asymmetries and imperfections in the gong. They also observed nonlinear behavior with the presence of subharmonics and identified the (0,1) and (1,1) modes as being the most important acoustically. McLachlan similarly studied small gongs and compared the spectra of cast bronze gongs with those of spun steel gongs [9]. He found that the intervals between modes are greatly dependent on the size of the boss and length of the rim.

Krueger et al. studied the ombak produced by a gong wadon [1]. Measurements with a microphone and a scanning laser were used to identify the resonance frequencies. Nonlinear behavior was observed in the presence of harmonics from the first axisymmetric mode. They concluded the interaction of the first harmonic with the second axisymmetric mode was the cause of the ombak. Driving the gong with sufficient amplitude at the first two axisymmetric mode

resonances produced audible beating. Figure 1.2 shows the beating phenomenon, where the beating frequency decreases over time. As a note, the fundamental (and by extension the harmonic) rises very slightly in frequency due to increased rigidity when displaced at high amplitudes and slowly restores as the amplitude decays. This moves the pitch of the harmonic further and then closer to the second mode frequency, which causes initially faster beating that slows over time [10].

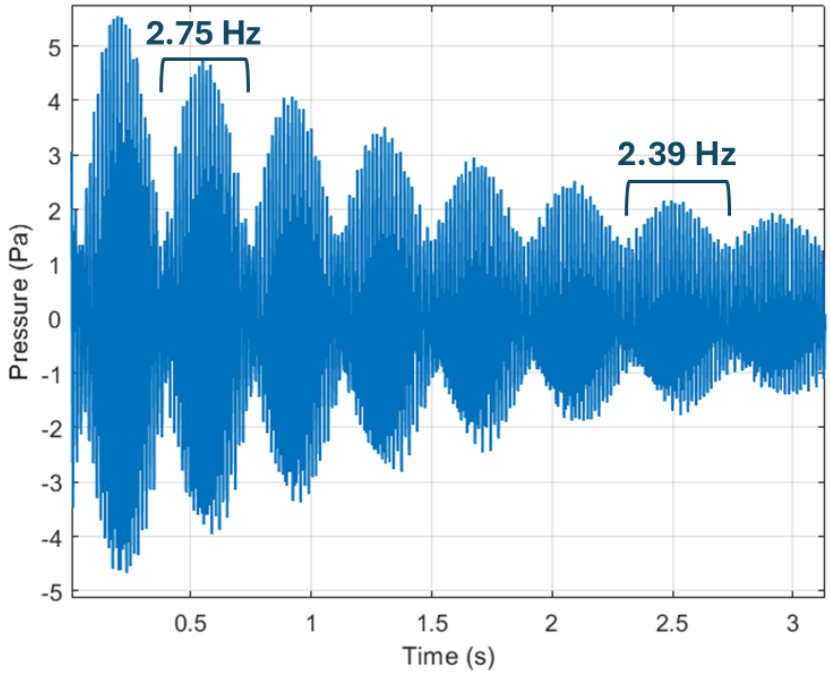

Figure 1.2 Time waveform for the struck gong wadon. The beating is clearly visible and its amplitude decays over time as the gong rings. The plot also shows a beating frequency of about 2-3 Hz, where almost 3 peaks fit within every second. It is also notable that the beating frequency decreases slightly over time.

1.3 Current Study

Although there is some understanding of the beating and modal behavior of the gongs, little has been done in terms of characterizing their directional behavior. This thesis will present a series of

studies performed in order to expand understanding of the directivity of gamelan gongs, and how it is informed by normal mode shapes, a cavity resonance, and a nonlinear harmonic.

The first study includes a comparison of the directivity and vibration patterns of the gong lanang with a bebende. The results of this study appear in several publications by Bellows [11, 12]. Directional behavior was measured, and surface scans were taken for each instrument. The author assisted with data processing and categorizing resonance behaviors. In most cases, the shape of the mode can inform the number and location of the lobes in a directivity pattern. It was also notable that the ordering of the modes was not the same for the lanang as it was for the bebende. Although the geometries of the gongs are similar, direct comparisons do not always hold between them.

Mathematical models were developed to replicate the measured directivity patterns of the gongs. Strong agreement was achieved between measurements and model in the low-frequency regime using a linear combination of monopoles and dipoles, and in higher frequencies using imposed mode shapes [11]. Another successful model applied a vibrating cap to a spherical shell with a defined aperture [13]. Curiously, both the measurements and shell model included a small range of omnidirectional behavior, where the mode shapes do not obviously match the observed directivity. An investigation of the Helmholtz resonance of the gong suggests its connection with this behavior.

Krueger et al. recognized a nonlinear harmonic as the cause of ombak and recreated the beating effect with the gong wadon by driving it at the first two axisymmetric resonance frequencies simultaneously [1]. However, no vibration or directivity measurements were taken while the beating was present. To determine the effect of beating on the acoustic radiation and to characterize the first harmonic, directivity and SLDV measurements were taken of the gong wadon driven at the first mode frequency and then driven at both resonances. This allowed for characterization of the nonlinear harmonic while isolated, and while interacting with the second mode.

Chapter 2

From Vibration to Radiation

To obtain an initial understanding of the acoustic radiation from Balinese gamelan gongs, both directivity and scanning laser Doppler vibrometer (SLDV) data were taken for a gong lanang and a bebende. Samuel Bellows conducted the measurement and the author assisted with processing and analyzing the data. The results have since been published (S. D. Bellows, D. T. Harwood, K. L. Gee, and M. R. Shepherd, "Directional characteristics of two gamelan gongs," The Journal of the Acoustical Society of America 154, 1921–1931 (2023)) and are crucial to the background and motivation of the other projects discussed in this thesis.

2.1 Methods

This study includes a comparison between the acoustic and vibrational data of a large and small gong. These data were taken with a directivity measurement system and a scanning laser Doppler vibrometer. Each of these two methods will be explained in the following sections.

2.1.1 Directivity Measurement System

The two gongs in this study were hung from their traditional frame and placed within a directivity measurement system (DMS) in the large anechoic chamber at Brigham Young University. Figure 2.1 shows the gongs in the rotational array of microphones that constitute the DMS. The array holds 36 12.7mm Larson Davis 40AE microphones separated vertically by 5 degrees. The array rotates azimuthally in 5-degree increments to create 2521 evenly spaced unique sampling positions (the top microphone remains fixed). A 37th microphone seen in the figure placed in front of the gongs serves as a reference. Relative calibration between the reference and the array provides normalization in post-processing.

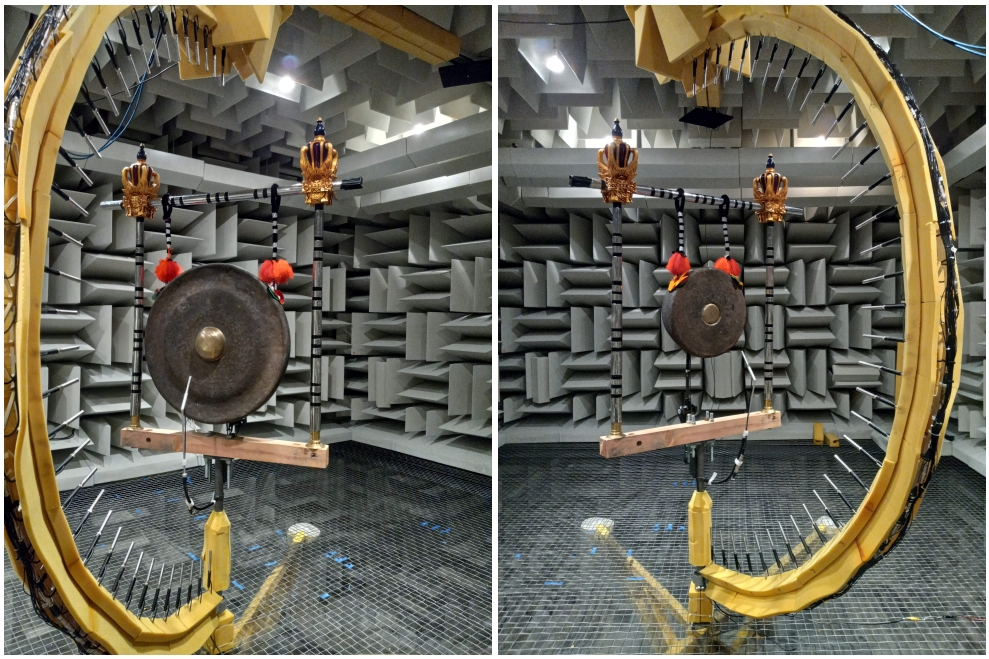

Figure 2.1 The gong lanang (left) and the bebende (right) in the directivity measurement system. The array of 36 microphones rotates 360 degrees around the gongs to produce the directivity plots. A reference microphone is seen in front of each gong for relative calibration with the other microphones. A shaker is mounted behind the gongs, not visible here [12].

A 5-second sine sweep input signal was sent to a shaker (LDS V203) to excite the gong over the audible bandwidth. This was repeated three times per array position to include averaging. Multiple measurements were taken with the shaker positioned on different locations behind the gong to ensure that all mode shapes were excited. More detailed methods regarding the shaker are explained in Appendix B. All measurements were taken with low-amplitude vibration; no beating from the gong was audible.

2.1.2 Scanning Laser Doppler Vibrometer

The vibrational patterns of the gong naturally influence its directivity, so it was essential to visualize these mode shapes in addition to the directional behavior. Using the same shaker at its various positions, an SLDV was used to scan the instrument. A fine grid of 977 points allowed for high spatial resolution in the resulting modal deflection patterns.

Upon completion of the measurements, the data were processed and examined. Power spectral density (PSD) plots allowed for the identification of resonances, and when the SLDV data were studied at these resonances the mode number could be determined. Then a comparison was made between the structural mode and the directivity pattern at the same frequency. Further comparisons were made between directivity and SLDV plots of the lanang versus the bebende to better understand the characteristics of each.

2.2 Results

Directivity balloon plots were made for 10 significant resonances for both the gong lanang and bebende. Surface velocity plots from the SLDV dataset are also provided. The directivity and vibration plots are taken from the recent publication by Bellows et al. [12].

2.2.1 Lanang

Figure 2.2 shows the directivity and mode shapes of the lanang at lower frequencies. The first row shows the directivity plots. Red regions represent areas of high pressure, or a 0 dB drop from the reference pressure, where green shows a 20 dB reduction of level. The 0 degree markings are directly above and in front of the gong. The operating mode shapes are shown on the second row with positive and negative phase shown in red and blue, with nodal lines in white.

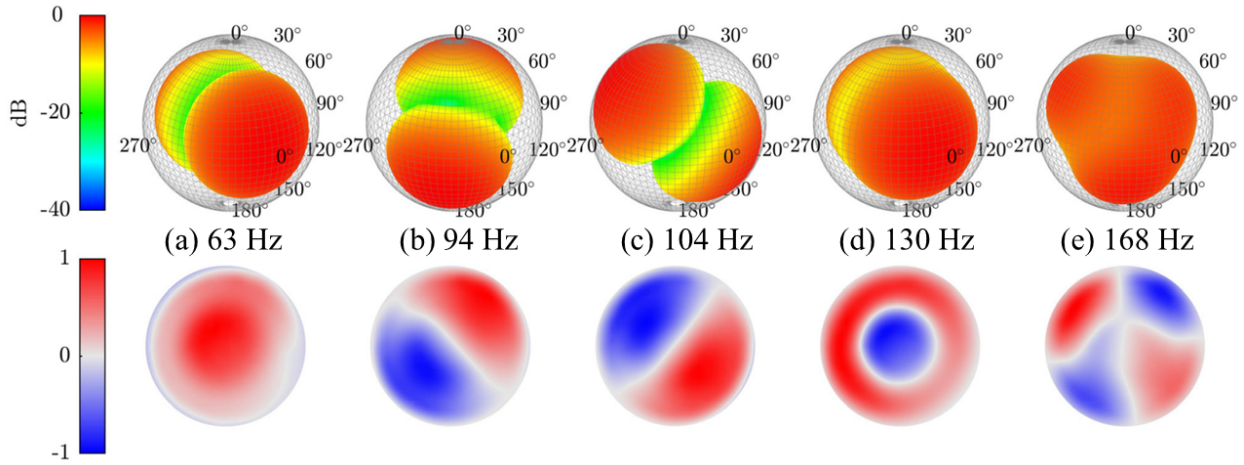

Figure 2.2 First set of directivity plots for the gong lanang. The top row shows the far field intensity of the gong as compared to a reference microphone. 0 degrees seen towards the bottom right of each plot represents the front face of the gong. The bottom row shows the operating mode shape of the gong's face for the same resonance frequencies. Dipolar behavior is seen in the first few modes with good agreement in nodal line location between mode shape and directional behavior. Note the exception with the omnidirectional behavior occurring in plot (e) where the two nodal lines are not visible [12].

Dipolar behavior is seen prominently in the first 4 resonances of the lanang. Lobing occurs in the front and back of the gong for the fundamental frequency, then moves to the sides. In Figure 2.2 (b) and (c), the angles of the (1,1) mode nodal lines match for both vibrational and acoustic data. Increasingly omnidirectional behavior is observed after the (1,1) modes. Plot 2.2 (e) resembles a monopole and appears to be the only directivity plot that does not visually relate to its mode shape .

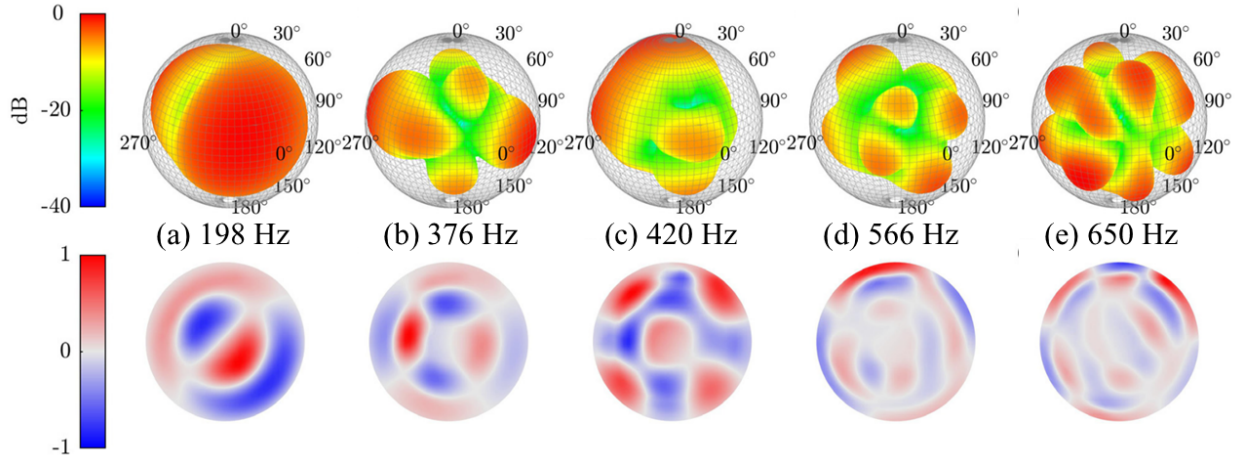

Figure 2.3 Second set of directivity plots for the gong lanang. The top row shows the far field intensity of the gong as compared to a reference microphone. 0 degrees seen towards the bottom right of each plot represents the front face of the gong. The bottom row shows the operating mode shape of the gong's face for the same resonance frequencies. More complex behavior occurs at higher frequencies. The nodal line does not appear to match between the (a) plots. There is still agreement between lobing in the directivity and antinodal regions on the outside of the operating mode shapes, seen especially in figures (b), (d), and (e) [12].

Higher frequency response of the lanang is shown in Figure 2.3. The (1,2) and (0,2) mode shapes are similar, and the directivity seen in 2.3 (a) appears related to 2.2 (d), matching in directional behavior fairly closely, though neither have the same clarity of nodal line as seen in 2.2 (a). Figure 2.3 (b) is also notable for the clear reflection of the mode shape in the directivity.

2.2.2 Bebende

Figure 2.4 shows the lower frequency response of the bebende. Dipole behavior is seen again with the (0,1) mode, but the directivities of the (1,1) mode degeneracies are not as intuitive as they were for the lanang as the lobing takes place more in the front and back than to the sides. There is good agreement between plots in 2.4 (d) as the directivity reflects the (2,1) mode behavior. Omnidirectional directivity occurs at the (0,2) mode resonance.

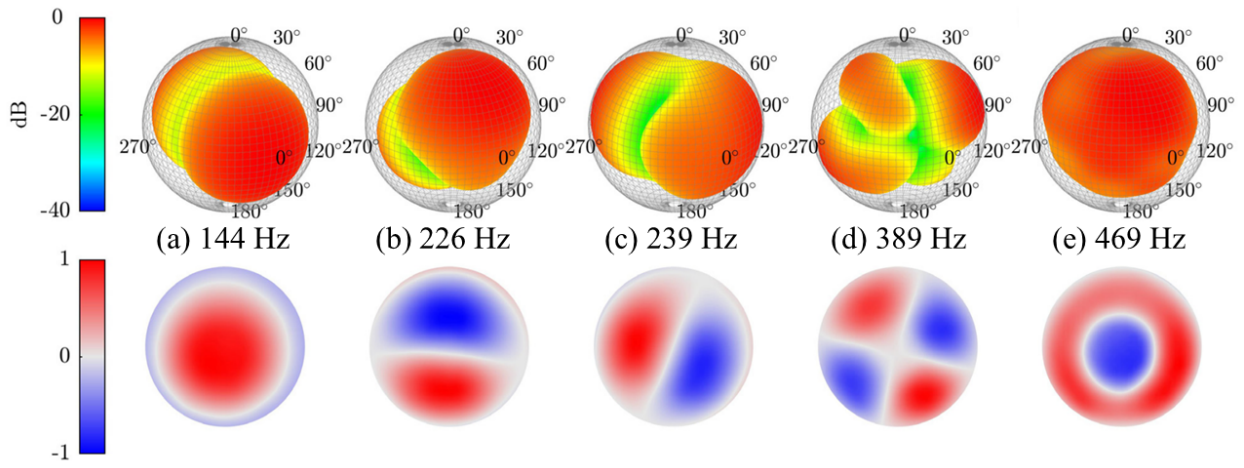

Figure 2.4 First set of directivity plots for the bebende. The top row shows the far field intensity of the gong as compared to a reference microphone. 0 degrees seen towards the bottom right of each plot represents the front face of the gong. The bottom row shows the operating mode shape of the gong's face for the same resonance frequencies. Dipolar behavior is seen again although the nodal line in the directivity of (b) and (c) does not cross the front face of the gong as it did for the lanang. Note the agreement between the plots in (d) and the omnidirectional behavior in (e) [12].

The link between the far-field radiation patterns and the operating deflection shapes is undeniable in Figure 2.5. The number and location of antinodal regions along the circumference of the gong correspond exactly to the location and number of lobes in the directivity plots. The white node lines match in location with the green regions of lower pressure. Figures 2.5 (d) and (e) show agreement between the directivity plots and their respective mode shapes in number and location on the front and even the sides.

2.3 Discussion

Our understanding of musical instruments is greatly enhanced by a study of their directivity patterns. The circular geometry of the gamelan gongs creates familiar structural vibration patterns that inform the intensity in the far field. The modal deflection shapes seen were comparable to the results of

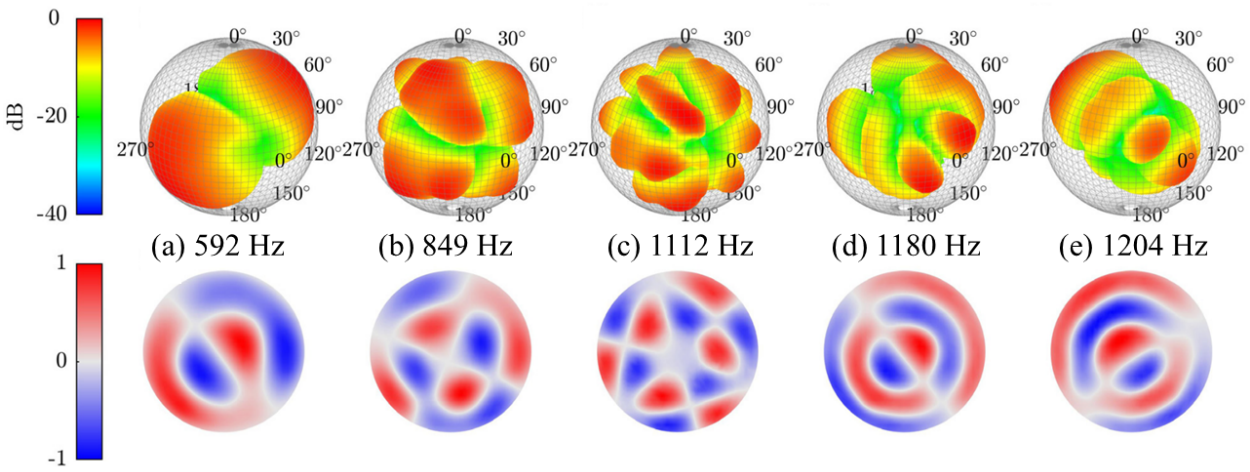

Figure 2.5 Second set of directivity plots for the bebende. The top row shows the far field intensity of the gong as compared to a reference microphone. 0 degrees seen towards the bottom right of each plot represents the front face of the gong. The bottom row shows the operating mode shape of the gong's face for the same resonance frequencies. Note the strong agreement between the number and location of lobes in the directivity plots with the antinodal regions along the circumference of the operating mode shapes [12].

Perrin, Rossing, and Fletcher [5,8]. There is good agreement between the structural vibration and the acoustic radiation patterns of the gongs in the data presented. Many plots demonstrate consistency in the placement and angle of nodal lines between vibrational and acoustic measurements. Because these data were taken on separate occasions, this consistency supports past conclusions about nodal lines being fixed in position due to the hand-crafted nature of the gongs [8]. Antinodal regions in the operating mode shape correspond to directivity lobes in both number and location. This is particularly clear in Figure 2.5, where every directivity plot resembles the vibrational pattern of the same frequency. Agreement between vibration and directivity occurs in all of the presented data with the exception of omnidirectional behavior which is present in some frequency bands.

The directivities of the gong lanang and bebende are similar in many respects, yet there are several key differences to note. The (1,1) mode is shown for the lanang in Figure 2.2 (b) and (c) and for the bebende in Figure 2.4 (b) and (c). The lanang directivity follows the pattern of the operating

mode shape, with lobing on the diagonals, while the bebende has stronger radiation in the front and back of the gong despite expected nodal lines along the frontal plane from the mode shape. The opposite is true with the (1,2) mode in Figure 2.3 (a) and Figure 2.5 (a) where the lanang has higher pressure towards the front and back and the bebende more closely resembles its mode shape with pronounced lobing on the sides. There is also a difference in pattern between Figures 2.3 (b) and 2.5 (b). Both plots match the (2,2) pattern, but the lanang shows uneven lobing to the sides and back while the bebende has a symmetric intensity towards the front.

The similarity in geometry between the gong lanang and the bebende implies comparability of their behavior; directivities and mode shapes intuitively occur in the same order, but at different frequencies. However, the data do not support a direct comparison as the directivity plots and mode shapes differ slightly from one gong to the other. An understanding of one does not imply knowledge of the other. Additionally, the mode ordering for the bebende is shifted from the ordering seen with the lanang. Table 2.1 shows the first seven modes of each gong in order of their respective frequencies. The (2,1) and (0,2) modes and the (3,1) and (1,2) modes appear in reversed order. These differences could result simply from the change of radius between the gongs or their non-uniform thicknesses due to their hand-made production.

The investigation by Krueger et al. [1] showed that the cause of the *ombak* (or beating) in the gong wadon is a non-linearly generated harmonic of the first axisymmetric mode interacting with the second axisymmetric mode. In other words, a doubling of the (0,1) mode lands near enough the (0,2) mode to create beating. This conclusion was also seen in the above study with the lanang and bebende. Table 2.2 shows the simple calculations that demonstrate why acoustic beating is audible from the lanang (one of the gong ageng) and not from the bebende. The lanang's modal resonances and harmonics create a beating of around 4 Hz while the frequency distance between the first two axisymmetric modes of the bebende is too great to produce beating.

Frequency	Lanang	Frequency	Bebende
63 Hz	(0,1)	144 Hz	(0,1)
94 & 104 Hz	(1,1)	226 & 239 Hz	(1,1)
130 Hz	(0,2)	389 Hz	(2,1)
168 Hz	(2,1)	469 Hz	(0,2)
198 Hz	(1,2)	536 Hz	(3,1)
276 Hz	(3,1)	592 Hz	(1,2)
426 Hz	(4,1)	692 Hz	(4,1)

Table 2.1 Comparison of mode order between the lanang and bebende. Notice the (2,1) and (3,1) modes appear to have switched with the (0,2) and (1,2) modes in the bebende and thus appear earlier than in the lanang.

Gong	(0,1)	Harmonic	(0,2)	Effect
Lanang	63 Hz	$63 * 2 = 126$ Hz	130 Hz	130-126 = 4 Hz Beating
Bebende	144 Hz	$144 * 2 = 288$ Hz	469 Hz	469-288 = No Beating

Table 2.2 Calculation of beating frequency. This demonstrates the presence or lack of acoustic beating in each gong. The first harmonic frequency is two times the fundamental and occurs near the (0,2) mode resonance in the gong lanang but not in the bebende.

The following two chapters contain studies of the back cavity of the gong and the beating of the gong. The cavity will be presented to explain the omnidirectional behavior seen near frequencies such as Figure 2.2 (e), which is not otherwise explained by its relative operating mode shape. This directivity study did not consider nonlinear behavior, that is, the harmonics could be calculated in Table 2.1 from the measured structural modes, but the harmonics themselves were not measured in the study. An intentionally nonlinear study of the gong discussed in Chapter 4 reveals more information about the harmonic that causes the acoustic beating and what it looks like in the far field.

Chapter 3

Cavity Exploration

To understand the influence of the cavity on the acoustic behavior of the gong, both experimental and numerical techniques were used. Recently, Bellows et al. developed a mathematical model using a vibrating cap on a sphere to predict the directional behavior of the gongs [13]. The model accurately predicts the lobes of the balloon plots, as well as the unexplained omnidirectional behavior seen previously. This model, as well as acoustic measurements, were used to explore the Helmholtz resonance of the back cavity of the gong lanang and provide better understanding of the omnidirectional behavior.

3.1 Methods

Helmholtz resonator theory, physical measurements, and a newly developed model each predicted a resonance of the back cavity of the gong. This section will describe the processes taken to obtain those resonances and the assumptions made.

3.1.1 Helmholtz Resonance Prediction

A Helmholtz resonator is related to a mass-spring system in that a volume of air acts like a stiffness with a narrower length through which the air oscillates, acting like a mass. As with a normal mass-spring system, it will resonate at a certain frequency, just like air blown across the mouth of a bottle. The Helmholtz resonance of several instruments has previously been studied, especially those with a tone hole, such as a guitar [14]. A Balinese gong is geometrically different from these instruments, or from a bottle for that matter, but the air-filled cavity behind the gong suggests a resonance nonetheless. "Neckless" Helmholtz resonators exist and studies have identified such resonators in unlikely places, including the body of some crickets [15]. Choosing to model the gong as a Helmholtz resonator provides a framework for an investigation of the cavity resonance. The equation that governs the Helmholtz resonance of a system is given as

$$f_H = \frac{c}{2\pi}\sqrt{\frac{S}{L'V}} \tag{3.1}$$

where f_H is the resonance frequency, c is the speed of sound in air, S is the surface area of the cavity opening, L' is the effective "neck" length of the resonator, and V is the volume of air inside it [5]. Sound speed was assumed to be $343 m/s$ and surface area was determined by measurement. The effective volume was calculated assuming only 3/4 the depth of the gong to allow space for the neck portion, using $V = \pi\, r^2 h$ with r being the radius of the face of the gong and h being the depth of the cavity. The remaining quarter depth was assigned to L, with $L' = 5L$. The dramatic increase between length and effective length is due to the nature of the resonator having an opening so much larger in area than the neck length, causing the true length to be much longer. These parameters provided a very rough estimate of f_H = 200.5 Hz, which was encouraging because Figures 2.2 and 2.3 indicate a possible resonance between 130 Hz and 198 Hz which is very close in frequency considering the several assumptions made. The purpose of using resonator theory here was not accuracy, but rather to gain intuition about the behavior of the gong.

3.1.2 Cavity Measurement

The Helmholtz resonance of the gong lanang was measured by placing a microphone in line with the rim of the gong in 9 different positions shown in Figure 3.1. A speaker was oriented to play diagonally into the back edge of the gong to reduce reflections out of the cavity. The cavity was excited by a 10-second sine sweep from 20-5000 Hz, covering the lower end of the audible bandwidth. This measurement provided data to produce power spectral density plots for each of the 9 positions, allowing observation of the resonance frequencies.

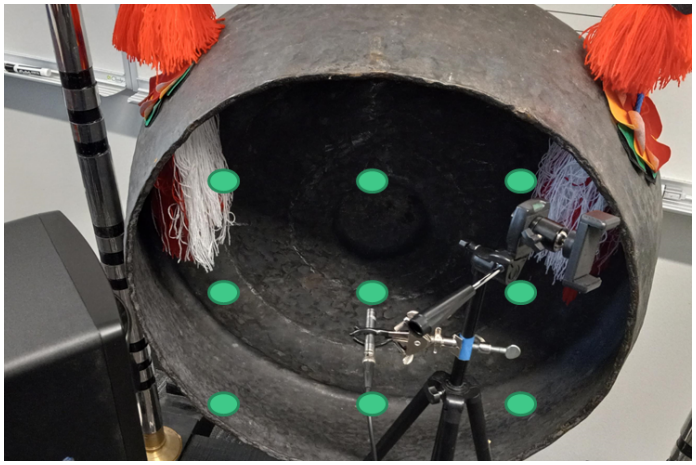

Figure 3.1 A sketch of the cavity measurement locations. This shows the location of 9 different measurement points taken while investigating the cavity resonance of the gong lanang. This is the effective "grid" used to create contour plots of the cavity pressure. The speaker is seen on the left and is oriented diagonally in relation to the gong.

3.1.3 Model Prediction

The mathematical model predicted a resonance for comparison with theory and measurement. Figure 3.2 shows the basics of the model which include a vibrating cap placed on a hollow sphere of radius a with an aperture placed opposite the cap. Γ_c shown in red represents the area of the cap, which includes the whole front face of the gong as seen in the representation on the left of the figure. Γ_s in blue is the area of the sides of the gong that wrap behind the circumference and

Γ_a is the aperture area. The size of the cap and aperture are defined by the half-angles μ_c and μ_a respectively. The position of the cap is defined as $\theta_c = \pi/2$ and $\phi_c = 0$, where the aperture is placed at $\theta_a = \pi/2$ and $\phi_a = \pi$.

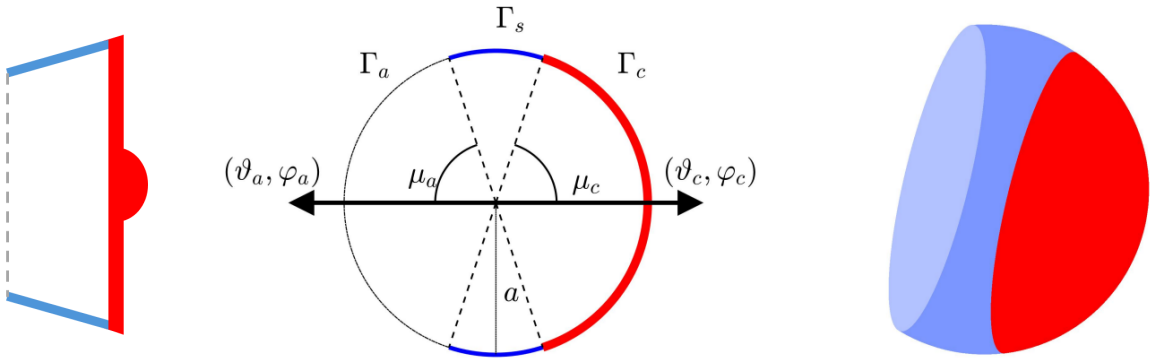

Figure 3.2 Model using a vibrating cap on a rigid sphere. A blue sphere of radius a is seen on the right and in the center with a red cap Γ_c located at (θ_c,ϕ_c) and an aperture Γ_a at (θ_a,ϕ_a). The size of the cap and aperture are defined by the half angles μ_c and μ_a respectively. The cap area Γ_c represents the front face of the gong as shown by the left diagram while the rest of the sphere Γ_s represents the long rim that wraps behind the gong and the aperture area Γ_a accounts for the air cavity behind the gong [13].

Assuming a position outside of the sphere, the equation

$$p(r,\theta,\phi,k) = \sum_{n=0}^{\infty} \sum_{m=-n}^{n} A_n^m h_n^{(2)}(kr) Y_n^m(\theta,\phi) \tag{3.2}$$

allows for the calculation of pressure at a given point and frequency, where A_n^m includes various velocity expansion coefficients (defined by Bellows et al. [13]), $h_n^{(2)}$ are the spherical Hankel functions of the second kind, and Y_n^m are the spherical harmonics of degree n and order m. A 30 by 30 cm grid was theoretically centered on the back aperture of the model with values of r only slightly larger than that of a in a way of recreating the previous physical measurement. The pressure at each of these locations was calculated from the above equation with frequencies from 1-1000 Hz. The resulting PSDs for several positions were examined to search for a resonance.

The publication of the model defines the parameters such as effective sphere radius a and cap half angle μ_c etc. and these were not changed in calculating the cavity resonance [13]. However, μ_a

was not defined as the published model only considers cases where $\mu_a = \mu_c$, although in reality the aperture angle would not physically be as large as the cap angle. To maximize the accuracy of the model, μ_a was determined by balancing angle ratios with area ratios as shown in Equation 3.3.

$$\frac{r_c^2}{r_a^2} = \frac{sin(\mu_c)^2}{sin(\mu_a)^2} \tag{3.3}$$

The r variables on the left-hand side represent the physically measured radii of the face (cap) and cavity (aperture) of the gong. The surface area of the front or back is obviously given by πr^2. To ensure that the scaling of the model matches the gong, the radii of the model should be given by $a * sin(\mu)$. Balancing the ratio of the model areas as shown above led to a half-angle μ_a slightly lower than μ_c, which matches the geometric shape.

3.2 Results

The calculated resonance frequency from the microphone measurements was 184 Hz. This is the highest amplitude peak shown in in the left plot of Figure 3.3, which displays PSD data from the center measurement. The two peaks just below it in frequency are likely a result of the (2,1) modal degeneracy resonances, one of which is seen in Figure 2.2 (e). Plotting the pressure from each of the 9 microphone positions at 184 Hz yielded the contour plot seen on the right of Figure 3.3. The overall trend of higher pressure in the center that decreased outward was reassuring, confirming the resonance did not correspond to the (2,1) mode, as there were no apparent nodes in the resulting pressure.

With the beforementioned gong parameters, the model calculated a resonance of 192 Hz which is seen overlaid with the measured PSD in Figure 3.4. A contour plot with perfect symmetry was also generated from the model at the resonance frequency, and agreement can be seen between it and the measured contour plot in Figure 3.3.

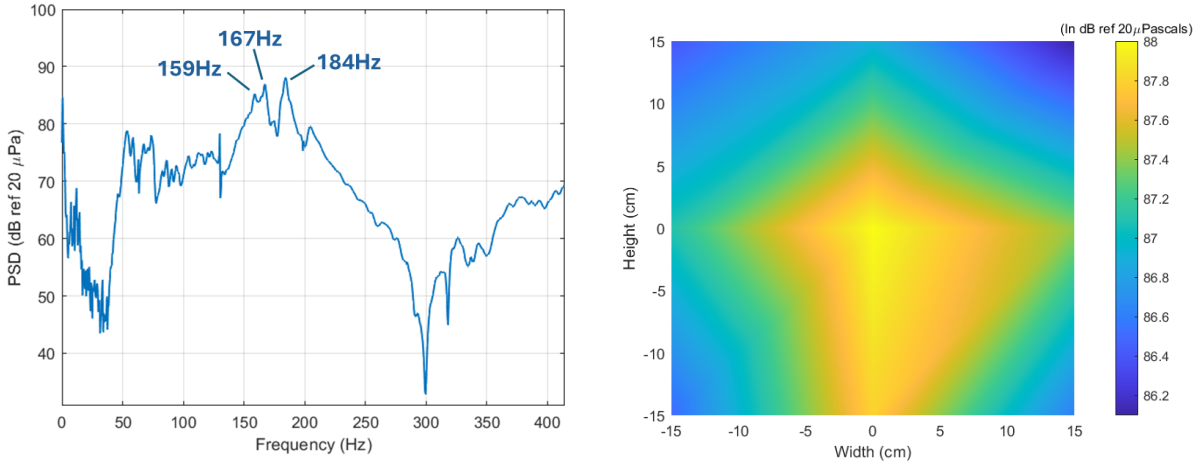

Figure 3.3 Power spectral density and contour plots for the gong cavity. A PSD plot is shown on the left for the center mic measurement behind the gong. The highest peak at 184 Hz shows the resonance frequency. Just below it are resonances likely due to the (2,1) structural mode degeneracies. A contour plot seen on the right was made using the 184 Hz resonance frequency and demonstrates the expected behavior of a Helmholtz resonator without any of the nodes that would be present in a (2,1) mode resonance.

3.3 Discussion

The agreement between the measured and modeled Helmholtz resonance frequencies is encouraging. The model was created without any intention of being used to calculate a cavity resonance, and yet it predicted one less than 10 Hz away from the measured resonance. Thus, the measured resonance of 184 Hz can be accepted with confidence. Additionally, the frequency range within which this resonance is occurring is the same as the omnidirectional behavior seen in the directivity plots of the lanang. Figure 2.2 (e) exhibits omnidirectional behavior that does not correspond to its mode shape and Figure 2.3 (a) radiates in most directions, lacking the expected nodal line in the front or back. The radiation from the bebende for the same modes is seen in Figures 2.4 (d) and 2.5 (a) and looks vastly different from that of the lanang. Microphone measurements and model predictions each show a cavity resonance between the frequencies of Figure 2.2 (e) and 2.3 (a). The influence of omnidirectional behavior appears visibly in Figure 2.2 (d), increases past (e), and seems to decrease

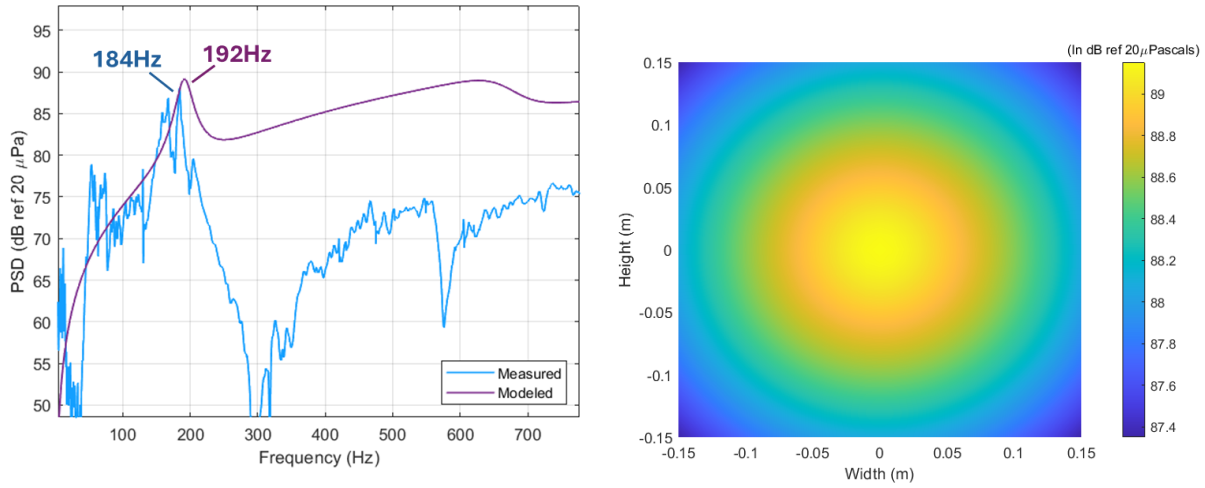

Figure 3.4 Power spectral density and contour plots for the modeled gong cavity. A PSD plot is shown on the left which superimposes the model results over the measured. There is strong agreement in the frequency location of the resonance with a difference of only 8 Hz. The structural resonances of the gong were not excited strongly by the speaker so it is not surprising it drops in amplitude after the Helmholtz resonance. A symmetric contour plot seen on the right was made using the model's resonance frequency and demonstrates the expected behavior of a Helmholtz resonator.

before Figure 2.3 (a). This behavior is in agreement with the decided cavity resonance of 184 Hz, concluding that the measured Helmholtz resonance interferes with the resulting far-field behavior of the gong at nearby frequencies.

The data shown here only represent the gong lanang from the Balinese gamelan. Data collected from the bebende cavity are presented in Appendix A. Physical measurements investigating the cavity were not anechoic and only included nine locations. Repetition of this measurement could provide better clarity as to the exact resonance and could better define the nearby peaks as certain structural resonances.

Chapter 4

Another Look at Nonlinear Harmonics

Previous studies have investigated the linear behavior of Balinese gongs in the far field, but in order to understand how the directivity could be influenced by the acoustic beating of these gongs, directivity and SLDV measurements were taken of the gong wadon while beating was audible. Audible beating requires the presence of a nonlinearly generated harmonic which has previously been unstudied. This chapter will characterize the vibration and radiation behavior of this harmonic. The contents of this chapter will be submitted as a proceedings article at the spring 2025 conference of The Acoustical Society of America.

4.1 Methods

In the nonlinear regime, a harmonic of the first mode of the gong wadon will form near the second mode and create audible beating. If the gong is driven sufficiently at the first mode, the harmonic will form an octave above it, and if the gong is driven at both modes, the frequency spacing between the harmonic and the second mode should cause acoustic beating. Testing these two conditions will allow for characterization of the harmonic both isolated, and interacting with the second axisymmetric mode resonance.

4.1.1 Directivity Measurement

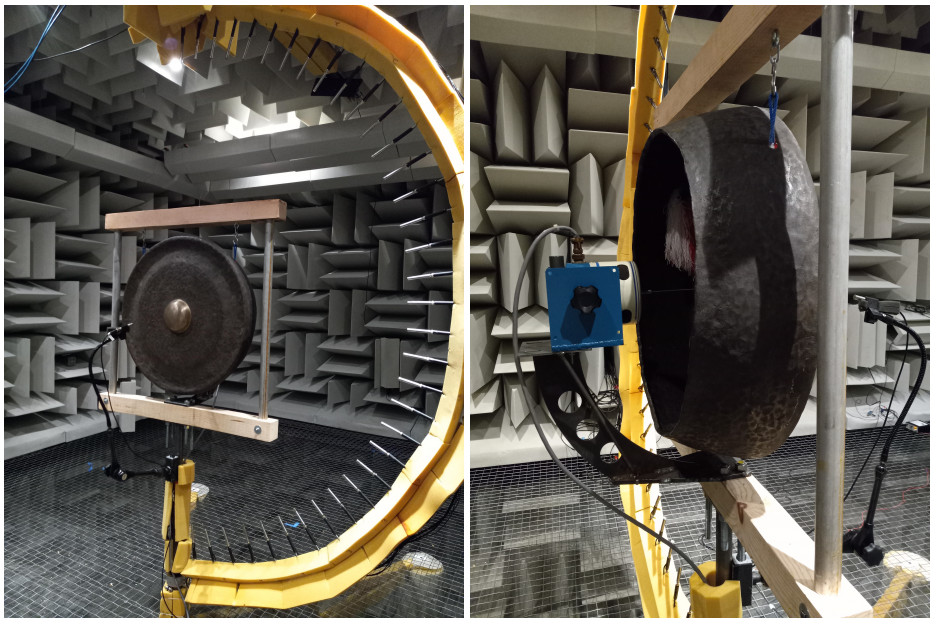

Figure 4.1 The gong wadon mounted in the directivity measurement system. A smaller frame allowed for better centering of the gong in the array. The rotational microphone array is seen in the 0 degree position. A shaker is set in the back and attached to the center of the gong.

The gong wadon was placed in the DMS with a reference microphone to plot high-resolution far-field behavior. Details of the DMS are explained in Section 2.1.1. A new frame seen in Figure 4.1 allowed for more precise centering of the gong in the array. A live musician test was initially recorded with a player striking the gong with its traditional mallet to isolate its natural beating sound from attached equipment such as the shaker and amplifier. Another measurement was taken of a low-amplitude sweep for comparison with the lanang directivity. The sweep duration was 3 seconds, ranged from 20-5000 Hz, and was repeated 3 times per array position to include averaging. PSD plots resulting from these measurements are shown in Figure 4.2. The PSD of the struck gong on the left is notable for the two clear resonances from the second mode and the harmonic. The resonance frequencies 121.5 Hz and 124.5 Hz cause the 3 Hz beating seen in Figure 1.2. The PSD

on the right shows the sweep data and the two axisymmetric mode resonance frequencies. Note that the resonances in the sweep data are slightly lower in frequency than those from the struck gong. This is due to the increased effective mass of the gong when the shaker is glued to the back. The resonances from the sweep data were chosen as the sine inputs for the harmonic study.

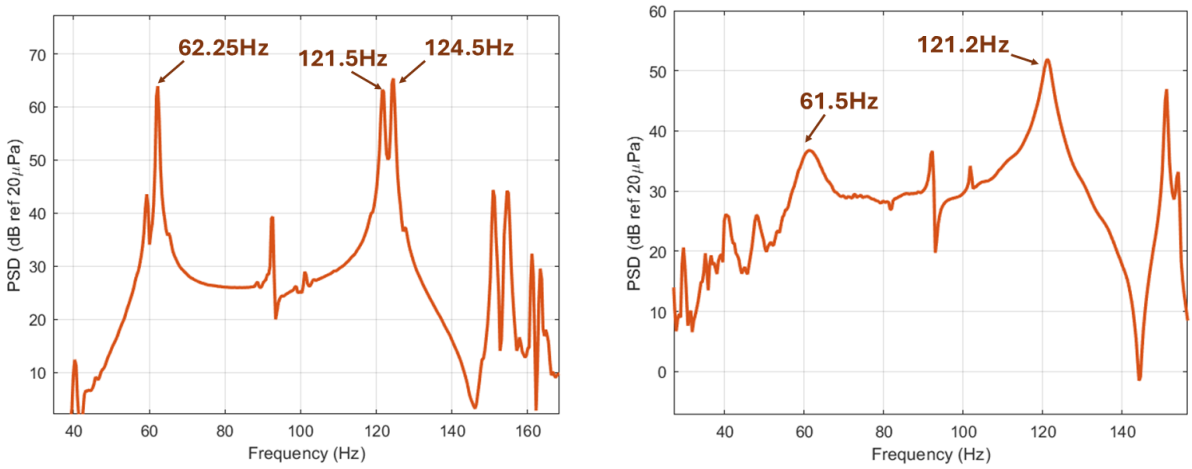

Figure 4.2 Power spectral density plots of the gong wadon. The plot on the left shows the gong's response when struck. The nonlinear affects are present and the proximity of the second mode at 121.5 Hz and the harmonic at 124.5 Hz is apparent. This causes the beating in Figure 1.2. Sweep data on the right shows the first two axisymmetric modes with slight frequency variations due to the attached shaker.

To investigate the nonlinear harmonic, the gong was first driven at the (0,1) resonance to isolate the harmonic. Then, in repetition of the methods used by Krueger, the gong was driven at its first two axisymmetric resonances simultaneously [1]. The gong's response to the two sine wave input is shown in Figure 4.3. The distance in frequency between the second mode and the harmonic is slightly smaller than before because of the resonance change with the shaker attached. This causes the beating waveform shown on the right to have a slower pulse than that seen in Figure 1.2. A Siglent function generator (SDG2042X) was used to output both the (0,1) and (0,2) resonance frequencies into an operational amplifier, which then transmitted the combined signal to another amplifier and then the shaker. The amplitude of the first mode was chosen to be 4 times that of

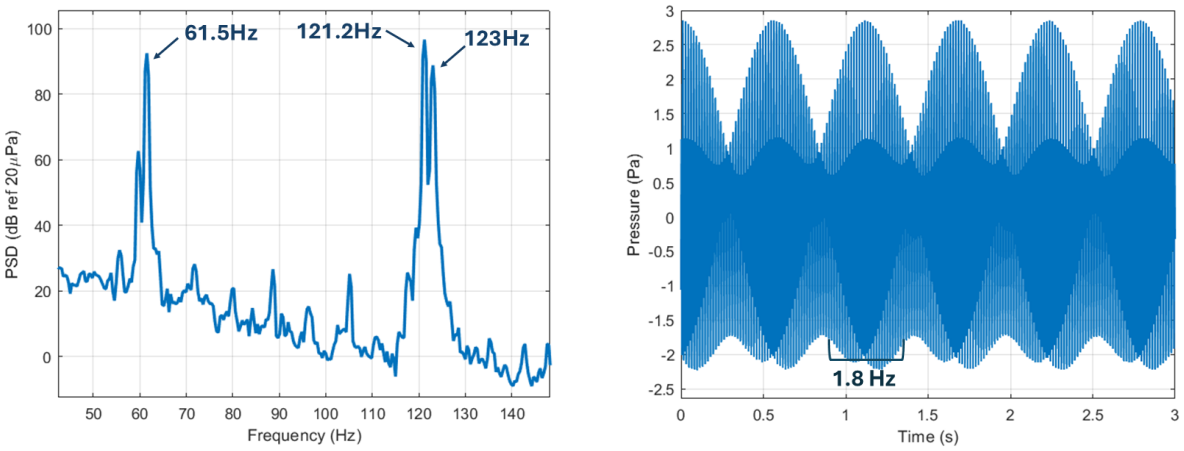

Figure 4.3 Power spectral density plot and beating waveform for the driven gong wadon. The PSD on the left shows the gong's response when driven at the 61.5 and 121.2 Hz resonances simultaneously. The nonlinear affects are present and the proximity of the second mode at 121.2 Hz and the harmonic at 123 Hz is apparent. The resulting 1.8 Hz beating is seen on the right. The frequency is slightly lower than before due to the shift in resonance frequency with the shaker attached behind the gong.

the second to achieve the most natural sound. A larger shaker (Ling Electronics) was used to drive the gong at sufficient amplitudes to introduce nonlinearity. It was centered on the boss to more efficiently excite the (0,1) and (0,2) modes.

4.1.2 Harmonic Distortion

It was noted early on that the harmonic of interest was present in the signal that was used to excite the gong. This was not desirable because the purpose of the study was to observe the harmonic as generated by the gong, and not the gong's response to being driven at the harmonic's frequency. Harmonic distortion from amplifiers constitutes a universal problem, and some studies have focused on removing distortion from the amplification process [16]. Figure 4.4 shows the microphone and signal spectra from a 61.5 Hz input, and from a combined input of 61.5 and 121.2 Hz.

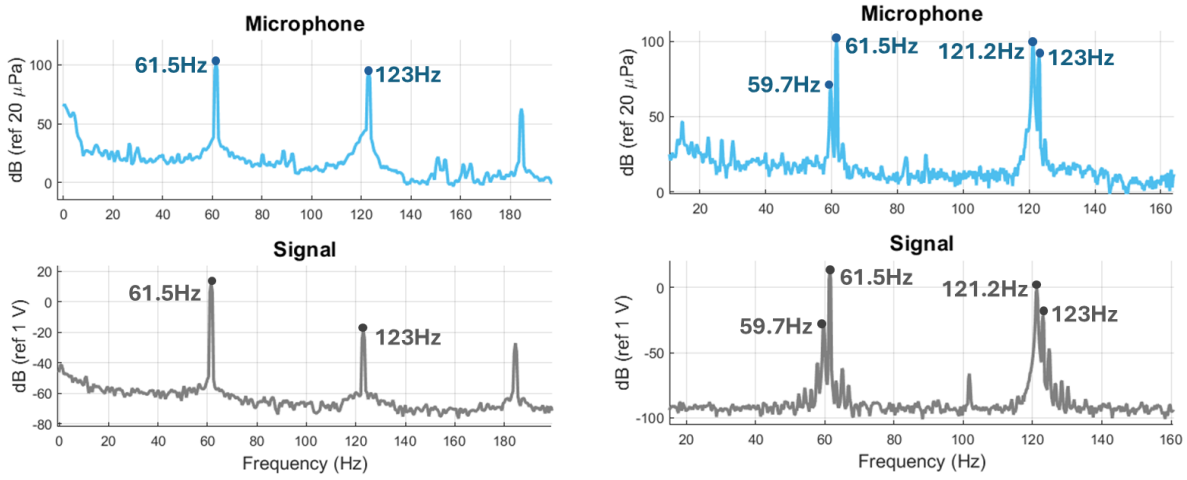

Figure 4.4 Frequency response of the amplifier-gong system. On the left are the spectra for a 61.5 Hz input and on the right are the specta for the combined 61.5 and 121.2 Hz input. Unwanted harmonics are present in the signal that could not be eliminated, but the harmonic of interest at 123 Hz is stronger in the microphone measurement than in the signal. This implies nonlinearity in the gong is contributing to the amplitude of the harmonic, thus validating the data set.

The signal spectra have multiple peaks resulting from distortion rather than the desired single or double sine input. Removing the amplifier from the system did not improve the results. Distortion can also occur from the AC current frequency in American outlets (60 Hz) being so near the amplifier input of 61.5 Hz. However, removing ground from the electrical system also did not affect the signal spectrum. As there is no way to complete a measurement without the signal generator itself, the op amp signal combiner, or the shaker, the distorted signal had to be tolerated. Comparison of electric and acoustic signals ensured that the measured harmonic was not purely a result of harmonic distortion from the amplifier. Figure 4.4 shows that nonlinearity from the gong itself contributes to the harmonic amplitude. In both cases, the signal experiences a 30 dB decrease between 61.5 Hz and its harmonic at 123 Hz while the microphone plots drop less than 10 dB from 61.5 to 123 Hz. A linear scale from the signal to the sound produced by the gong does not hold. This implies a significant portion of the harmonic's amplitude as recorded by the microphone is

contributed by the nonlinear effects of the gong which suggests that the desired phenomenon is present in the measurement.

4.1.3 Scanning Laser Measurement

An SLDV scan of the gong was also taken with a low amplitude sweep, single sine wave, and combined sine wave inputs. Each measurement consisted of a square data grid of 437 equally spaced points covering the front face of the gong. The first scan was a 1 second sweep input from 20 to 1000 Hz and showed the expected mode shapes of the gong. Additional scans with the 61.5 Hz input and then combined 61.5 and 121.2 Hz input allowed for the structural presence of the harmonic both isolated and in combination with the (0,2) mode. The vibrational behavior was then recorded at the harmonic frequency and compared with that of the (0,2) mode shape and the directional behavior of the harmonic.

4.2 Results

The directivity of the first two axisymmetric modes and the harmonic of the first mode were taken and compared with the operating mode shape data from the SLDV, similar to what was done in Chapter 2. The first two axisymmetric modes were comparable to those of the gong lanang seen in Figure 2.2 (a) and (d). The directivity of the harmonic from the struck gong data is shown in Figure 4.5. In this case, the 0 degree marks represent the top and the right side of the gong. The array position in Figure 4.1 shows 0 degrees in the azimuthal direction. The axial, median, and frontal plane behaviors are colored green, magenta, and blue, respectively. Immediately it is apparent that the directional behavior of the harmonic matches that of the second axisymmetric mode from Figure 2.2 (d). There is a faint nodal line that can be seen in the green axial plane outline, and the majority of the radiation tends towards the front and back of the gong.

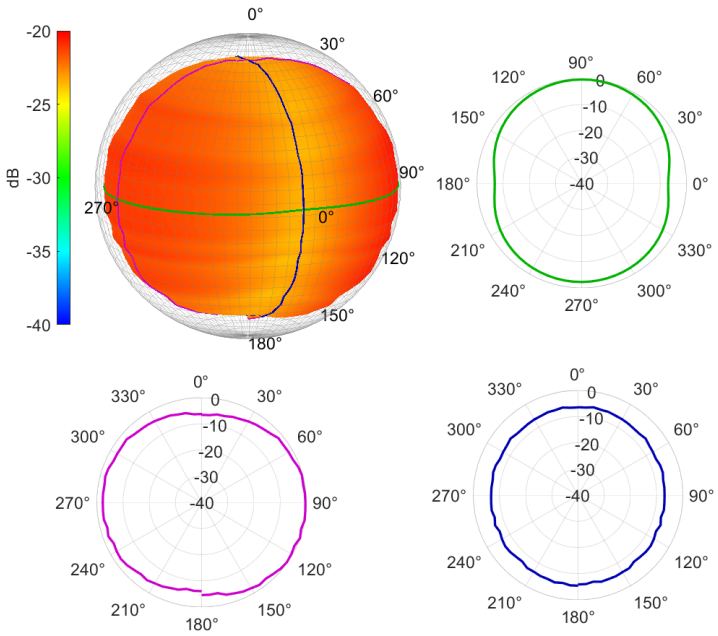

Figure 4.5 Directivity plot of the harmonic. This data was taken as the gong was struck with the traditional mallet. The directivity is shown in the upper left, where 0 degrees marks exactly above and to the right of the gong. The behavior of the axial plane is shown in green, the median plane in magenta, and the frontal plane is outlined in blue.

The directivity plot of the struck gong in Figure 4.5 shows how the harmonic resembles the (0,2) mode behavior. This was not only true for the struck measurement, but when the gong was excited by a 61.5 Hz signal and then a combination of 61.5 and 121.2 Hz, the behavior of the harmonic was identical. Although the measurement conditions differed and the resonance frequencies shifted, the harmonic and second mode from all tests appeared as seen in Figure 4.5.

Data from the laser scan showed similar results. Figure 4.6 shows the vibrational behavior of the gong at its fundamental and harmonic resonances. This scan was taken while the gong was driven at 61.5 Hz. The operating mode shape of the fundamental is shown in Figure 4.6a and demonstrates (0,1) mode behavior as expected while the harmonic at 123 Hz in Figure 4.6b vibrates like the (0,2) mode. The scan in which the gong was driven at both resonances simultaneously was not as clear

(possibly because the laser scanner had difficulty with the acoustic beating constantly changing the vibration amplitude) but showed the same results, where the (0,1) resonance behaved as expected and both the harmonic and second axisymmetric mode vibrated in the (0,2) pattern.

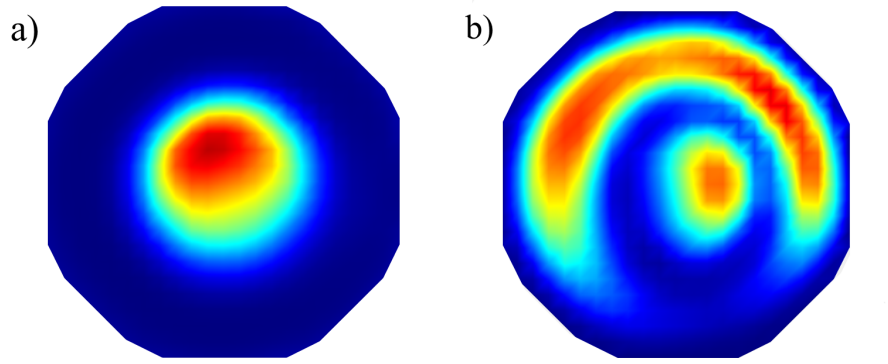

Figure 4.6 Vibrational behavior of the (0,1) mode and its harmonic. Here, red regions represent areas of maximum displacement where blue shows minimum displacement. This data was taken while driving the gong at 61.5 Hz. The fundamental mode behavior is seen in a), with (0,2) behavior seen in b), the harmonic at 123 Hz. These are comparable to Figure 2.2 (a) and (d) respectively. The asymmetry in the plots could result from slight shaker misalignment or non-uniform thickness of the gong.

4.3 Discussion

It was not anticipated to see the directional behavior of the harmonic match so closely with that of the second axisymmetric mode. They each have their own resonances at different frequencies which are visibly and distinctly separate in the PSD plots. Some modal degeneracies studied previously were close in frequency and shared similar directivity plots due to their common mode, but were always distinct, often with lobes being shifted by some angle. Proximity in frequency has not caused identical directivity behavior before.

The plots could be identical because the harmonic distortion causes the shaker to simply drive the gong near the (0,2) mode, which results in (0,2) mode directivity. This is unlikely because the

amplitude of the harmonic is much higher when measured from the gong than from the signal as seen in Figure 4.4. There is nonlinearity present, which should cause the harmonic to at least influence the nearby mode if it truly behaves differently. Additionally, the directivity of the harmonic was the same for both struck and driven measurements. Distortion had no effect on the strike measurement, and the far-field behavior is very closely tied to the operating mode shape as studied in Chapter 2. If the harmonic has the same directivity across all measurements, it is reasonable to assume the vibrational data are also the same (although it would be impractical to take a laser scan of a player measurement). With these considerations, it is not valid to assume that the vibrational data are identical due to distortion when the directivity data without distortion are also identical. Therefore, the behavior seen in the driven measurements can be observed without too much concern about distortion.

There are two other proposed explanations for the behavior of the harmonic. Nonlinearity produces the harmonic at $2f_0$, displacing the gong and creating tension forces there. Energy from the system is now being applied at that frequency and could be considered a force that drives the gong near the (0,2) mode resonance, causing the observed (0,2) behavior at both the harmonic and second mode frequencies. This is similar to the distortion argument above, with the important change that the gong creates this force naturally. Another possibility is a nonlinear superposition of modes. Nonlinear normal modes (NNMs) can be quite complicated, where different energy levels or displacement amplitudes can cause one mode to behave as a linear combination of one or more higher-order modes [17]. Indonesian gong-making tradition could have found a way to unknowingly take advantage of NNMs and encourage the harmonic of the fundamental to behave as the second axisymmetric mode. The nonlinearity could produce a fundamental with minimal contributions from other modes while producing a harmonic that both vibrates with exactly the same pattern of the second axisymmetric mode and occurs within just a few hertz of it, enhancing the characteristic beating effect of the gong.

Chapter 5

Conclusion

The Balinese gamelan is at the heart of music in Bali. The instruments in the gamelan have not received as much attention as Western instruments, but have been the subject of some studies that observed their vibrational behavior [5, 8, 9]. Studying these instruments helps keep their culture alive by increasing awareness of and interest in them. Research on the gamelan has also led to a better understanding of these instruments and motivated the development of several models that have demonstrated the application of theoretical principles to represent real instruments.

In 2010, David Krueger et al. studied the beating effect present in the large gongs of the gamelan [1]. The studies described in this thesis focused on the directivity of the gamelan gongs, a previously unstudied characteristic of the gongs. The measured directivity was studied in connection with the vibrational behavior of the gong, its cavity resonance, and its nonlinear behavior.

5.1 Comparison of Two Gongs

The directivity and vibrational behavior was studied for both a large and a small gong. Directivity measurements were taken with a rotational array of microphones in an anechoic chamber, and operating mode shapes were measured with a scanning laser Doppler vibrometer. The directivity

and mode shape of 10 significant resonances were presented and discussed for each gong. The first harmonic of the fundamental was calculated to demonstrate the presence of beating in the gong lanang and not the bebende [1].

A comparison was made between the directivity and modal characteristics of a large and small gong, which revealed significant differences. The vibration and radiation patterns of the two gongs are similar, but not always the same, even for the same mode shape. The ordering of the modes is also different between the gongs; one gong cannot predict the other's behavior.

An understanding of the directivity characteristics of the gongs allows for further development and testing of models. Dipolar behavior is notable in the lower frequencies of both gongs and a model has since been created using spherical harmonic and multipole expansions to predict directivity patterns [11]. The operating mode shape of a resonance can inform the resulting directivity pattern at higher frequencies. Placement and quantity of directivity lobes often correspond to antinodal sections on the mode shape. Another successful model has been developed that imposes mode shapes on a rigid sphere to preserve their effect on the resulting directivity [13].

5.2 Cavity Resonance

The far-field behavior of the gong is influenced by its operating mode shape. This is true for most resonances, yet the directivity shown in Figure 2.2 (e) is omnidirectional and does not relate to the modal behavior. A mathematical model consisting of a vibrating cap on a hollow, open rigid sphere (Figure 3.2) likewise predicted directivity patterns with more omnidirectional behavior. An investigation of the cavity resonances for both the gong lanang and the mathematical model revealed that the Helmholtz resonance occurs in the same region as the omnidirectional behavior.

The Helmholtz resonance equation (Eq. 3.1) was applied with reasonable parameters and predicted a resonance near 200 Hz, which motivated physical measurement. A microphone placed

in various locations behind the gong measured a resonance of 184 Hz while application of the model calculated 192 Hz. The unique approach of each of these methods gives confidence in the value of 184 Hz as the Helmholtz resonance of the gong lanang, which occurs directly between the two radiation patterns that have otherwise unexplained directivity behavior. The Helmholtz resonance appears to directly influence the far-field directivity of neighboring structural resonances.

5.3 Nonlinear Study

The directional behavior of the gong has been characterized in the linear regime, but the nonlinear harmonic responsible for the acoustic beating of the gong has not previously been studied [1]. Directivity and scanning laser measurements were taken of the gong driven at its fundamental mode and at a combination of its first two axisymmetric modes to observe the nonlinear harmonic both isolated and occurring next to the second mode.

Directivity measurements of the nonlinear harmonic matched those of the second mode in every instance. SLDV data further revealed the harmonic to behave the same as the second axisymmetric mode. Harmonic distortion was noted, but seems an unlikely culprit for the (0,2) mode behavior, as the radiation of a player measurement agreed with all other tests. Nonlinearity causes displacement and tension forces at the harmonic frequency, and these forces could simply drive the gong near the second axisymmetric mode to generate the observed behavior. Nonlinear normal modes (NNMs) could also explain the behavior, as they include a linear combination of higher-order modes. The gong may have been crafted so that the harmonic of the fundamental contains mostly contributions from the (0,2) mode. This would enhance the observed beating as the two frequencies responsible for it share both vibrational and directional behavior.

Appendix A

Bebende Cavity Measurement

The data presented in Chapter 3 only included measurements of the lanang. The bebende was also measured, but the results did not match the narrative of the thesis. This is a brief summary of the study.

The same methods as explained before were applied. A quick calculation using the Helmholtz resonance equation determined a rough estimate of 265 Hz. Using the previous assumptions in balancing the ratio of surface areas to determine the aperture half angle μ_a, the model predicted nearly the same at 267 Hz.

Physical measurement proved slightly more challenging for the bebende. Two resonance frequencies competed for highest amplitude. The left side of the figure below shows the PSD of the back cavity, with two frequencies near 85 dB. Depending on the microphone location, one would surpass the other in magnitude. The determining factor was an analysis of the contour plots. The right side of the figure shows a contour plot at 231 Hz that matches expectations, very similar to Figure 3.3. Another contour plot for the 211 Hz resonance showed intensity focused in the top left corner, decreasing outwards. This implied a resonance of the (1,1) mode shown in Figure 2.4, making 231 Hz appear to be the reasonable candidate for the Helmholtz resonance . This value

does not match the predicted values as well as with the lanang, but is not far enough to cause alarm considering the assumptions made in the predictions.

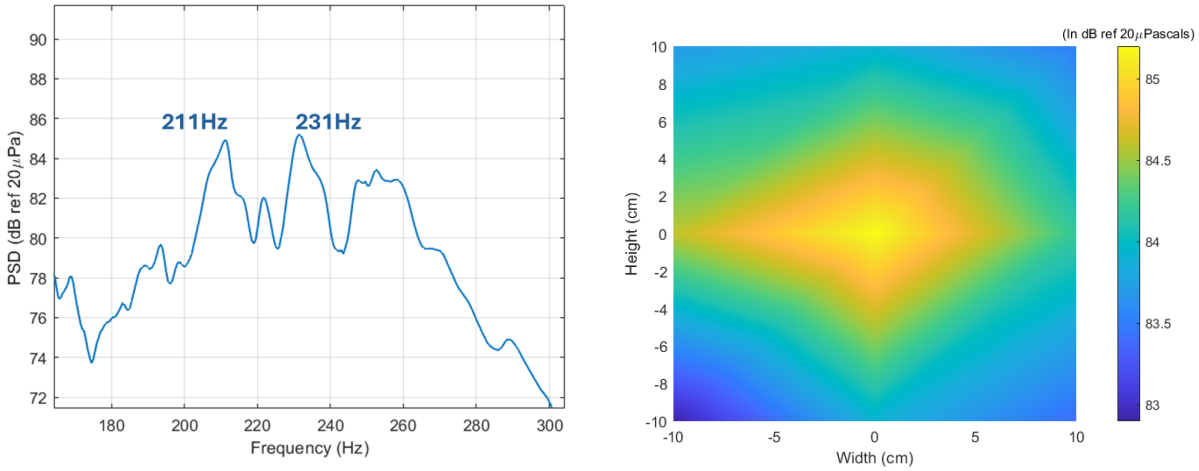

Figure A1 Power spectral density and contour plot for the bebende cavity. A PSD plot is shown on the left for the center microphone measurement of the bebende cavity. There are two distinct peaks at 211 and 231 Hz, where the former appeared to be a (1,1) structural mode resonance, and the latter behaved more like the expected resonance. A contour plot seen on the right was made using the resulting resonance frequency of 231 Hz.

Now, comparing the value of the cavity resonance to Figure 2.4 seems to reveal a lack of connection between the resonance and omnidirectional behavior . An argument can be made that the (1,1) directivities may not behave the same as in Figure 2.2 because they are influenced by the resonance. Front-to-back radiation could be related to a cavity resonance, but this does not answer the question of why the omnidirectional behavior occurs in Figure 2.4 (e), far away in frequency from the measured resonance. Scaling down the geometry of the gong can cause unforeseen complications in the behavior. As discussed in Section 2.3, a direct linear comparison is not appropriate, and the behaviors between the large and small gongs may not be intuitively related. These complexities were not investigated thoroughly, and the question is left open for future work.

Appendix B

Shaker Methods

Figure B1 Examples of shaker positions for the original directivity study. On the left, the shaker is attached with putty to the side of the bebende in order to excite the mode shapes that have nodal lines through the center. On the right, the case where the shaker is positioned on the boss of the gong lanang to excite its axisymmetric modes is shown.

The shaker used in the original directivity measurement (LDS V203) was attached via putty to the back of the gong lanang and bebende. The putty was a sufficient force to keep the shaker attached to the gong, as all measurements were taken with low-amplitude excitation. The position of the "stinger" (the thin rod connecting the shaker body to the gong) varied in all measurements to ensure that all mode shapes would be excited. The figure above shows different positions of the stinger on both the lanang and bebende.

A larger shaker (Ling Electronics) was used in the more recent study of the harmonic with the gong wadon. Two stands were constructed to allow the shaker to be mounted behind the gong. One stand (seen in the first picture below) attached to the new smaller frame (better seen in Figure 4.1) that was used in the anechoic chamber. The other stand seen below could be placed on the ground and adjusted to the right height to be used while the gong hung in its traditional (and transportable) frame. The shaker was secured to the stands with screws for stability.

The stinger included with the larger shaker terminates in a threaded portion. This end was threaded and glued into a small flat disk that was then glued to the back of the gong. The larger surface area of the disk allowed for a more secure connection to the gong. The stinger was always glued to the center of the gong, on the boss, so that the axisymmetric modes would be excited more efficiently. Gorilla Super Glue was used to attach the stinger to the gong and isopropyl alcohol was helpful in removing the glue from the gong and stinger when the measurements were completed.

Figure B2 Two methods for mounting the shaker. The anechoic measurements required a stand that would not block the path of the rotating microphone array, so it attached directly to the frame underneath the gong as seen on the left. The stand on the right sits on the floor and can be adjusted to the desired height to center the stinger on the boss of the gong. This configuration was more convenient for SLDV measurements. In this image the stinger was comprised of two separate pieces connected by a threader piece. Any loosening of this piece would introduce noise to the system and white foam seen here was tied down to the piece to reduce the noise. Eventually this configuration was abandoned for a new stinger seen in the picture below.

Figure B3 A single stinger piece connecting the shaker to the center of the gong wadon. The stinger rod ends in threading that was attached to a small round plate about the size of a nickel. This plate was then glued to the gong. The best stinger connection and position were achieved by setting the gong and shaker in the anechoic configuration seen in the left picture above. After gluing the stinger to the center of the gong, it would be pushed forward slightly to displace the gong before being tightened in place. The constant pressure from the weight of the gong would provide an adequately strong attachment for the higher amplitude tests.

Bibliography

[1] D. W. Krueger, K. L. Gee, and J. Grimshaw, "Acoustical and vibrometry analysis of a large Balinese gamelan gong," The Journal of the Acoustical Society of America **128,** 8–13 (2010).

[2] Communication with Dr. Jeremy Grimshaw, Associate Dean of the BYU School of Music.

[3] Musicador, "Soniccouture Balinese Gamelan,", 2007.

[4] J. Meyer, "The sound of the orchestra," Journal of the Audio Engineering Society **41,** 203–213 (1993).

[5] N. H. Fletcher and T. D. Rossing, *The physics of musical instruments*, 2nd ed. (Springer Science & Business Media, 1998).

[6] A. Chaigne, M. Fontaine, O. Thomas, M. Ferre, C. Touzé, and E. C. de la Hunière, "Vibrations of shallow spherical shells and gongs: a comparative study," In *Proc. Forum Acusticum (Sevilla)*, (2002).

[7] M. E. Jones, K. L. Gee, and J. Grimshaw, "Vibrational characteristics of Balinese gamelan metallophones," The Journal of the Acoustical Society of America **127,** EL197–EL202 (2010).

[8] R. Perrin, D. P. Elford, L. Chalmers, G. M. Swallowe, T. R. Moore, S. Hamdan, and B. J. Halkon, "Normal modes of a small gamelan gong," The Journal of the Acoustical Society of America **136,** 1942–1950 (2014).

[9] N. McLachlan, "Finite element analysis and gong acoustics," Acoustics Australia **25,** 103–108 (1997).

[10] Communication with Dr. Matthew Allen, Professor in the BYU College of Engineering.

[11] S. D. Bellows, D. T. Harwood, K. L. Gee, and T. W. Leishman, "Low-frequency directional characteristics of a gamelan gong," In *Proceedings of Meetings on Acoustics*, 50 (2022).

[12] S. D. Bellows, D. T. Harwood, K. L. Gee, and M. R. Shepherd, "Directional characteristics of two gamelan gongs," The Journal of the Acoustical Society of America **154,** 1921–1931 (2023).

[13] S. D. Bellows, M. R. Shepherd, K. L. Gee, and T. W. Leishman, "Modeling the sound radiation of gamelan gongs using analytic rigid spherical models," In *Proceedings of Meetings on Acoustics*, 51 (2023).

[14] M. Elejabarrieta, C. Santamaria, and A. Ezcurra, "Air cavity modes in the resonance box of the guitar: the effect of the sound hole,", 2002.

[15] T. Jonsson, B. D. Chivers, K. Robson Brown, F. A. Sarria-S, M. Walker, and F. Montealegre-Z, "Chamber music: an unusual Helmholtz resonator for song amplification in a Neotropical bush-cricket," Journal of Experimental Biology **220,** 2900–2907 (2017).

[16] H. H. Jang, K. W. Choi, and D. I. Kim, "Novel frequency-splitting SWIPT for overcoming amplifier nonlinearity," IEEE Wireless Communications Letters **9,** 826–829 (2020).

[17] R. Kuether, L. Renson, T. Detroux, C. Grappasonni, G. Kerschen, and M. Allen, "Nonlinear normal modes, modal interactions and isolated resonance curves," Journal of Sound and Vibration **351,** 299–310 (2015).

Index